Available online at www.sciencedirect.com
ScienceDirect
Catalysis Today 121 (2007) 130–139
CATALYSIS TODAY
www.elsevier.com/locate/cattod

Enantioselective hydrogenation over immobilized rhodium diphosphine complexes on mesostructured materials

Adrian Crosman, Wolfgang F. Hoelderich *

Department of Chemical Technology and Heterogeneous Catalysis, Universiry of RWTH-Aachen, Worringerweg 1, 52074 Aachen, Germany

Available online 27 December 2006

Abstract

New heterogeneous chiral catalysts were prepared from rhodium diphosphine complexes [Rh(P–P)COD]Cl ((P–P) = diphosphine ligand and COD = cyclooctadiene), and Al–MCM-41, Al–MCM-48, and Al–SBA-15, respectively. Impregnation of the mesoporous Al–MCM-41, Al–MCM-48, and Al–SBA-15 with the organometallic complexes in dichloromethane led to strongly bonded hydrogenation catalysts. The catalysts were characterised with XRD, FT-IR and MAS-NMR, as well as thermoprogrammed desorption of ammonia, thermogravimetric analysis, and nitrogen sorption experiments. The hydrogenation of dimethyl itaconate, methyl α-acetamidoacrylate, and methyl α-acetamidocinnamate were studied as test reactions. The immobilized catalysts showed high activities and excellent chemo- and enantioselectivities. Up to 98% e.e., >99% conversion and 99% selectivity were observed in the case of studied prochiral olefins. The catalysts could be reused without a loss of catalytic activity. Leaching of the homogeneous complex out of the mesoporous framework was not observed.

Keywords: Immobilization; Rhodium; Diphosphine; Al–MCM-41; Al–MCM-48; Al–SBA-15; Asymmetric; Hydrogenation

1. Introduction

Chiral synthesis has received much attention because of the rapid growth of the pharmaceutical and agrochemical market in the last decades [1–3]. For economic, environmental, and social reasons, the trend towards the application of optically active compounds is undoubtedly increasing. Among the various methods for selective production of single enantiomers, asymmetric catalysis is the most attractive method from the atom economic point of view [4,5]. Homogeneous asymmetric catalysis has made tremendous progress over the last decades and is well recognized in this field. This fact has also been expressed by dedicating the Nobel Prize Award for chemistry in 2001 to Noyori, Sharpless and Knowles [6].

Transition metal catalyzed reactions are among the most efficient routes to obtain compounds with high enantiomeric purities. Especially hydrogenations are of particular industrial relevance because of the high efficiencies that can be obtained with a relatively small environmental impact [5]. Among others, complexes of rhodium, ruthenium, and more recently iridium, have been used successfully for catalytic asymmetric hydrogenations of prochiral olefins [4,7,8]. The use of an iridium complex as hydrogenation catalyst in the critical synthesis step for the preparation of grass herbicide ‘‘Metolachlor’’ shows that the use of these catalysts is not limited to the laboratory scale [9].

Rhodium based complexes have long been investigated in asymmetric hydrogenations, achieving high reaction rates and excellent enantioselectivities under optimized reaction conditions [10,11]. Among these ligands, chiral diphosphines are known to perform excellent results in this type of reaction for more than 30 years [12,13]. However, homogeneous asymmetric catalysts are not used to their full extent, which for a large part is due to problems in separation and recycling of the expensive chiral catalysts. Although these problems can be ignored on a small lab scale, they are of a decisive importance for the economical and technological viability of a large scale production. Furthermore, even if the activity and selectivity of homogeneous catalysts is exceptionally high, toxicological and environmental problems should also be taken into account.

Since the late 1970s, many approaches have been published by academic and industrial researchers to ‘‘heterogenize’’,

* Corresponding author. Tel.: +49 241 8026560; fax: +49 241 8022291.
E-mail address: hoelderich@rwth-aachen.de (W.F. Hoelderich).

0920-5861/$ – see front matter © 2006 Published by Elsevier B.V.
doi:10.1016/j.cattod.2006.11.023

"immobilize" or "anchor" homogeneous catalysts on solid supports [14–16]. Many excellent reviews have emerged in recent years, which describe in detail the synthesis and use of polymer-supported catalysts [17,18] and catalysts on inorganic carriers [19–21], or both [22–24]. However, the catalytic properties of these immobilized catalysts have shown an enormous variation and in many cases were significantly below those of the homogeneous analogues. Since the reasons for these differences in performance are usually not understood, it is still of interest to test different immobilization methods and supports in order to get a systematic picture of positive and negative effects.

Mesoporous molecular sieves have received much attention in the field of catalysis, especially for their use as supports. Ion exchange, catalytic and adsorptive properties of molecular sieve materials are based on the existence of acid sites which arise from the presence of accessible hydroxyl groups associated with tetrahedral framework aluminum in a silica framework. Our research was focused on the use of M41S and SBA-15 type materials as carriers, which are characterized by a well defined pore structure and high surface area, offering new opportunities for the immobilization of large homogeneous catalyst species without any modification of their chemical structure [25–29]. MCM-48 has been investigated to a lesser extent even though it should be more applicable as a catalyst or adsorbent due to its three-dimensional pore architecture. The recently discovered pure silica phase, designed SBA-15, has long range order, large monodispersed mesopores (up to 50 nm) and thicker walls (typically between 3 and 9 nm) which make it more thermally and hydrothermally stable than the M41S type materials. Unfortunately, as the pure silica SBA-15 is synthesized in strong acid media (2 M HCl solution), incorporation of framework aluminum into SBA-15 by direct synthesis seems to be impossible because most aluminum sources dissolve in strong acids. Previous studies have shown that aluminum can be effectively incorporated into siliceous SBA-15 via various post synthesis procedures, e.g. by grafting aluminum onto SBA-15 wall surfaces with anhydrous $AlCl_3$ or aluminum isopropoxide in nonaqueous solutions, or sodium aluminate in aqueous solutions followed by calcination [30,31].

Herein, we present a very straightforward way for the immobilization of rhodium diphosphine complexes. This heterogenization is based on an ionic interaction between the negatively charged Al–M41S or Al–SBA-15 framework and the cationic rhodium of the organometallic complex. Furthermore, activity of the obtained catalysts in the enantioselective hydrogenation of different prochiral olefins was investigated.

2. Experimental

It is well known that Rh-complexes containing diphosphines are very sensitive to moisture and oxygen. Phosphines can be easily oxidized under such conditions, and then loose their catalytic activity. Considering these reasons, all the experiments involving diphosphines, rhodium diphosphine complexes and immobilized complexes were carried out in argon filled Mbraun LabStar glovebox or using standard Schlenk-type techniques. In order to remove all adsorbed water molecules, the solid supports were calcined overnight at 300 °C prior to the immobilization of organometallic complexes. Moreover, all used solvents were dried and degassed using well-known standard methods.

2.1. Preparation of the mesostructured materials

Al–MCM-41 was prepared according to a slightly altered method reported by van Hooff [32]. In a 250 mL PE flask, 10.5 g tetraethylammonium hydroxide (TEAOH, 40 wt.%, aqueous), 0.21 g $NaAlO_2$ and 50 g H_2O were mixed together and stirred at room temperature for 1 h, followed by the addition of 10 g tetradecyltrimethylammonium bromide. The resulting mixture was stirred for 4 h. Then, 15.23 g Ludox-HS 40 were added dropwise over a period of 1 h, followed by vigorous stirring at ambient temperature for 4 h. The crystallisation took place at 105 °C for 6 days. After the third and fifth day, pH was adjusted at 10.2 using CH_3COOH (10 wt.%, aqueous). After crystallisation, the solid phase was recovered by filtration and well washed with water. The white material was dried at 120 °C overnight, followed by calcination in static air at 540 °C for 6 h (heating rate 1 °C/min).

Al–MCM-48 was prepared as follows: in a 500 mL PE flask, TEAOH (40 wt.%, aqueous), $NaAlO_2$ and water were stirred at room temperature for 1 h, followed by the addition of cetyltrimethylammonium bromide. Then, Ludox HS-40 was added dropwise over a period of 1 h, followed by vigorous stirring for 4 h. The molar composition of the gel was as follows: Si/Al = 40, TEAOH/Si = 0.3, surfactant/Si = 0.45 and water/Si = 60. The crystallization was performed at 120 °C for 8 days using a Teflon lined autoclave. After the second, fourth and sixth day, pH was adjusted at 10.8 using CH_3COOH (10 wt.%, aqueous). The final solid reaction product was extracted from the autoclave, filtered, washed with distilled water and dried at 120 °C overnight. Finally, the solid was calcined at 540 °C for 6 h (heating rate 1 °C/min).

For SBA-15 synthesis, 20 g of amphiphilic triblock copolymer, poly(ethylene glycol)-block-poly(propylene glycol)-block-poly(ethylene glycol) (average molecular weight 5800, Aldrich), was dispersed in 150 g of water and 600 g of 2 M HCl solution while stirring, followed by the addition of 42 g of tetraethyl orthosilicate to the homogeneous solution with stirring. This gel mixture was continuously stirred at 40 °C for 6 h, and finally crystallized in a Teflon-lined autoclave at 90 °C for 3 days. After crystallization the solid product was filtered, washed with deionized water, and dried in air at room temperature. The material was calcined in static air at 550 °C for 24 h to decompose the triblock copolymer and obtain a white powder (SBA-15) [27]. This white powder is used as the parent material to produce aluminum-containing material denoted as Al–SBA-15.

Silica SBA-15 (10 g, 166.5 mmol Si) was dispersed in 250 mL of dry hexane containing 0.85 g (4.1 mmol Al) aluminum isopropoxide. The resulting suspension was stirred at room temperature for 24 h, and afterwards the powder was filtered, washed with dry hexane, and dried at 120 °C in air. This solid Al–SBA-15 was then calcined in static air at 550 °C for 6 h (heating rate 1 °C/min) [30].

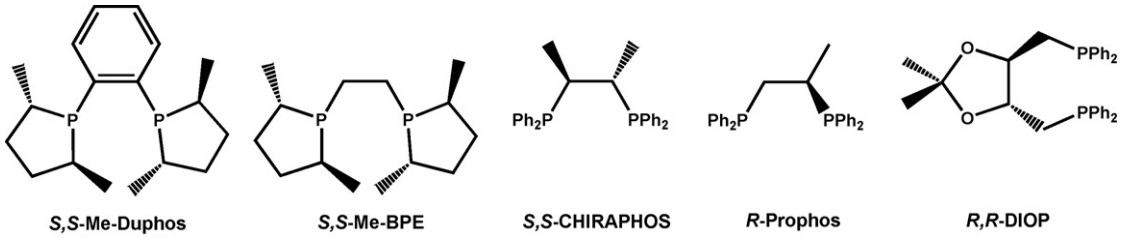

Fig. 1. Used diphosphine ligands.

2.2. Preparation and immobilization of the rhodium diphosphine complexes

In a Schlenk tube under Ar, $[CODRhCl]_2$ (0.075 mmol) was dissolved in 20 mL CH_2Cl_2 and then a solution containing the corresponding diphosphine (0.165 mmol diphosphine; *S*,*S*-Me–DUPHOS *R*,*R*-Me–BPE, *S*,*S*-CHIRAPHOS, *R*-PROPHOS or *R*,*R*-DIOP; Fig. 1) was added. The resulting mixture was stirred at room temperature for 6 h, and then the solvent was eliminated under reduced pressure. The obtained solid was dried under vacuum overnight.

For each diphosine ligand, an organometallic complex was prepared according to the previously described method. In order to immobilize Rh–diphosphine-complexes, 1 g mesostructured material (Al–MCM-41, Al–MCM-48 or Al–SBA-15) was suspended in 9 mL CH_2Cl_2 and stirred at room temperature for 1 h. The Rh–diphosphine-complex (0.15 mmol) was dissolved in 1 mL CH_2Cl_2 and added to the solid/CH_2Cl_2 suspension. The reaction mixture was stirred at room temperature for 24 h followed by solvent evaporation under reduced pressure. The recovered solid was Soxhlet extracted with MeOH for 24 h, in order to remove any residual free Rh complex. The absence of the homogeneous complex in the upper aliquot was checked by ICP-AES analysis as well as by FT-IR spectroscopy. The final material was vacuum dried at room temperature overnight. The heterogeneous catalyst has a pale yellow color similar to the color of the homogeneous complex. Fig. 2 presents a simple sketch of the immobilized rhodium diphosphine complexes.

2.3. Catalyst characterization

XRD powder diffraction patterns were collected on a Siemens Diffractometer D5000 equipped with a secondary monochromator, a variable diaphragm V 20 and a nickel filter using Cu Kα radiation (wavelength 1.5406 Å), the angle speed was 0.02 °/min. Bulk elemental chemical analyses were done with inductive couple plasma atomic emission spectroscopy (ICP-AES) on a Spectroflame D (Spectro Analytic Instrument). Nitrogen adsorption/desorption isotherms at liquid nitrogen temperature were measured on a Micromeritics ASAP 2010 instrument. The samples were pre-outgassed at 150 °C. Pore diameter and specific pore volume were calculated according to the Barrett–Joyner–Halenda (BJH) theory. The specific surface area was obtained using the Brunauer–Emmett–Teller (BET) equation.

FT-IR analyses were done on a Nicolet Protégé 460, equipped with an evacuable furnace cell with KBr windows containing the sample wafer. Without using a binder, the samples were pressed into self-supporting wafers, which, after being mounted onto the sample cell, were dried at 200 °C and 10^{-3} mbar for 16 h. Adsorbed pyridine spectra were taken using a Nicolet Protégé 460 equipped with an evacuable furnace cell with KBr windows, containing the sample wafer. The samples were pressed into self-supported wafers, which, after being mounted onto the sample cell, were dried at 200 °C and 10^{-3} mbar for 16 h. After cooling down the cell to 50 °C the background spectra was recorded. Spectra were always collected as an average of 200 runs with 0.5 cm^{-1} definition. The pyridine adsorption was carried out equilibrating the catalyst three times with pyridine vapors at 50 °C, by shutting off the cell from vacuum and opening a pyridine containing flask to the cell. After 60 min of evacuation a spectrum was recorded. The desorption of the probe molecule was successively monitored stepwise, by evacuating the sample for 60 min at 50, 100 and 200 °C and cooling to 50 °C between each step, to record the spectrum.

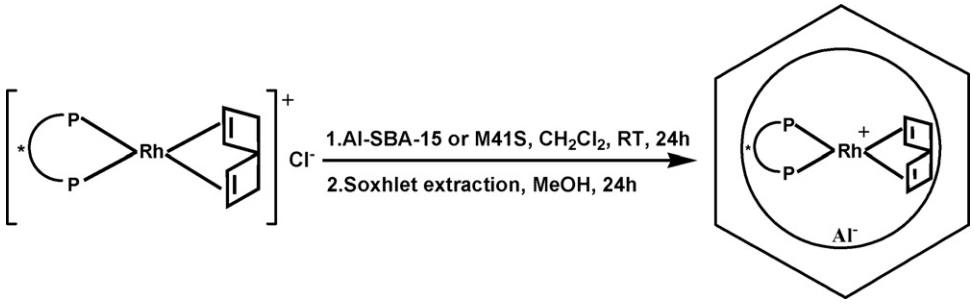

Fig. 2. Immobilization of rhodium diphosphine complexes.

For thermogravimetric analysis a Netzsch 209/2/E equipped with a STA 409 controller was used. The heating rate was 5 °C/min, and α-Al_2O_3 was used as reference material. Temperature programmed desorption of ammonia was measured on a TPDRO 1100 apparatus from CE Instruments. First, the materials were calcined for 2 h at 500 °C under argon, followed by ammonia loading at 100 °C (3% NH_3 in argon, 2 h). Subsequently, the system was purged with argon for 2 h, and then NH_3 was desorbed by heating with a heating rate of 25 °C/min to 900 °C under flowing argon. For comparison of loaded and pure carries home build apparatus was used. These experiments were performed at atmospheric pressure using a flow type fixed-bed adsorber. Prior to the TPD experiments, the materials were calcined at 200 °C in dry nitrogen for 8 h, loaded with ammonia at 100 °C, and purged with nitrogen until a stable baseline formed. The desorption was done in the temperature range 100–400 °C at a heating rate of 5 °C/min under nitrogen flow.

The solid-sate NMR spectra were recorded on a Bruker DSX 500 spectrometer, equipped with a 2.5 mm CP/MAS probe-head. In the case of the ^{31}P-MAS NMRspectra, 5000–10,000 transients gave satisfactory signal-to-noise ratios. The samples were rotated at 20,000 Hz. The spectra were recorded at room temperature (296 K) and aqueous 85% H_3PO_4 was used as the external standard.

2.4. Catalytic tests

2.4.1. Homogeneous hydrogenations

In a glove box, a Fischer–Porter bottle was charged with the corresponding amount of substrate, anhydrous, degassed MeOH, and the rhodium diphosphine complex (0.1 mol%). After five vacuum/H_2 cycles, the tube was pressurized to a pressure of 3 bar H_2. The reactions were allowed to stir at 20–25 °C for 24 h. Complete conversion to product was confirmed by GC as well as ^{1}H and ^{13}C NMR. The reactions were concentrated on a rotavap, and the residue passed through a short SiO_2 column (EtOAc/hexane, 1/1) to remove the catalyst. Without further purification, the enatiomeric excesses were determined directly on an aliquot of the crude products thus obtained.

2.4.2. Heterogeneous hydrogenations

In a glove box, a Fischer–Porter bottle was charged with the corresponding amounts of substrate, anhydrous, degassed MeOH, and immobilized rhodium disphosphine complex. After five vacuum/H_2 cycles, the tube was pressurized to a pressure of 3 bar H_2. The reactions were allowed to stir at room temperature for 24 h. The aliquots were passed through a 20 μm PTFE filter and submitted to GC analysis without any further treatment. Conversion, selectivity and enantioselectivity were determined via chiral capillary GC using the appropriate chiral column. The heterogeneous catalysts were recycled using standard methods (the catalysts were recovered by filtration or centrifugation, washed with 5 mL MeOH, dried overnight under vacuum at room temperature and reused in the next cycle at the same substrate/catalyst ratio).

3. Results and discussion

The X-ray powder diffraction of the Al–MCM-41, Al–SBA-15 and Al–MCM-48 showed the characteristic hexagonal or cubic structure, respectively. Al–MCM-41 showed a sharp peak ascribed to (1 0 0) reflection of the hexagonal structure of mesopores at $2\theta = 2.44°$, corresponding to $d_{1\,0\,0} = 3.045$ nm. Besides the strong peak, weak ones ascribed to (1 1 0) and (2 0 0) reflections at $2\theta = 4.2°$ and 4.9°, $d = 1.68$ and 1.48 nm, respectively, were observed. XRD pattern of Al–MCM-48 sample revealed the presence of a sharp peak ascribed to (2 1 1) reflection of the cubic structure at $2\theta = 2.28$ °, corresponding to $d_{211} = 3.327$ nm. A second peak corresponding to the (2 2 0) reflection was observed at $2\theta = 2.76$ °. Al–SBA-15 showed a well-resolved pattern with a prominent peak at 0.8 °, and two peaks at 1.4 ° and 1.6 ° 2θ which match well with the pattern reported for SBA-15. The XRD peaks can be indexed to a hexagonal lattice with a $d_{(1\,0\,0)}$ spacing of 1 1 0 Å, corresponding to a large unit cell parameter $a_0 = 127$ Å ($a_0 = 2d(1\,0\,0)/\sqrt{3}$). However, for carrier materials the intensity of the reflections essentially did not change upon loading the carrier with the organometallic complexes, nor after a catalytic cycle, showing that the mesoporous structures were not affected by the incorporation of the catalyst.

Elementary analysis results for Rh, Si and Al are presented in Table 1. During the immobilization in dichloromethane, the color transfer from the orange solution of organometallic complex to the white solid demonstrated a high degree of immobilization. However, upon extraction with methanol, which in contrast to the nonpolar dichloromethane adsorbs strongly on the solid surface, the adsorbed (non bounded) complex desorbs from the silanol groups due to a competitive reaction with the polar alcohol. Determined rhodium content was generally between 0.03 and 0.07 mmol/g, while the theoretic content was 0.15 mmol Rh/g.

A special case is the trial of immobilization of rhodium diphosphine complexes on an all silica materials (Fig. 3). In case of all silica SBA-15, the solid material had an orange color and a Rh content of 0.07 mmol/g was found after the first immobilization step in dichloromethane. After the extraction with methanol, the entire amount of organometallic complex was washed off and the final material had again the original white color. No rhodium was detected in ICP-AES analyses of this sample. However, in the case of aluminum containing mesostructured materials the orange color obtained after the immobilization of the rhodium complexes in dichloromethane

Table 1
Elemental analysis for parent and loaded materials

Sample	Rh theoretic (mmol/g)	Rh real (mmol/g)	Si/Al theoretic	Si/Al real
Al–MCM-41	–	–	40	37.9
RhDuphos/Al–MCM-41	0.15	0.07	40	38.2
Al–MCM-48	–	–	40	37.1
RhDuphos/Al–MCM-48	0.15	0.08	40	37.9
Al–SBA-15	–	–	30	28.3
RhDuphos/Al–SBA-15	0.15	0.04	30	29.3

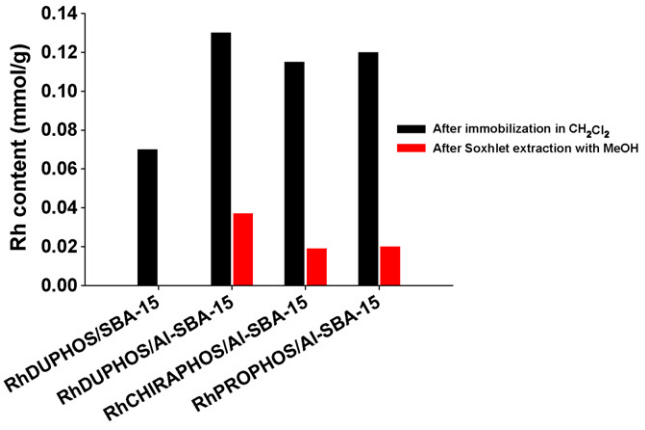

Fig. 3. Rhodium content after immobilization in CH_2Cl_2 and extraction in MeOH.

Table 2
Aluminum content before and after immobilization

Sample	Al/Na	Al/Rh
Al–MCM-41	0.99	–
RhDuphos/Al–MCM-41	1.19	5.14
RhChiraphos/Al–MCM-41	1.07	9.12
Al–MCM-48	0.98	–
RhDuphos/Al–MCM-48	1.19	4.81
RhChiraphos/Al–MCM-48	0.98	9.12

is clearly maintained even after extraction in methanol. These results clearly showed the influence of the network tetrahedral aluminum. This tetrahedral aluminum is negatively charged and a counter cation is present for charge neutralization. In case of Al–MCM-41 and Al–MCM-48 the negative charge is neutralized by a sodium cation. Table 2 presents the aluminum/sodium molar ratio before and after immobilization. As expected, after immobilization this ratio is increasing due to the ionic exchange of sodium with the cationic rhodium complex.

N_2 sorption isotherms were measured for the pure carrier and for all immobilized complexes, respectively. Fig. 4 and Table 3 present a comparison of sorption isotherms and textural characteristics for pure and loaded samples. In all the cases, these isotherms presented the characteristic form of mesoporous materials. It can be easily remarked that the N_2 adsorbed/desorbed volume was higher in the case of pure carrier than in the case of immobilized complexes.

Table 3
Textural characteristics of parent and loaded materials

Sample	Surface area ($m^2\ g^{-1}$)	Pore volume ($cm^3\ g^{-1}$)
Al–MCM-41	1190	0.97
RhDuphos/Al–MCM-41	1092	0.77
Al–MCM-48	1211	1.04
RhDuphos/AlMCM-48	1082	0.81
Al–SBA-15	467	0.92
RhDuphos/Al–SBA-15	397	0.78

N_2 sorption isotherms of the supported catalysts showed a decrease of the surface area and of the mesopore volume of ca. 15% compared to the corresponding parent material. For example, the BET surface area was found to decrease from 1190 m^2/g for the carrier material to 1092 m^2/g for RhDuphos/Al–MCM-41, with a corresponding decrease in mesopore volume from 0.97 to 0.77 cm^3/g. These results indicated that the complex was most likely deposited inside the pore system of the mesostructured materials.

The infrared spectra of the loaded materials revealed the presence of bands attributed to the characteristic organic structure of the diphosphine complexes (Fig. 5). Although these bands are weak and not characteristic enough to resolve a structure, several typical bands could be distinguished, as for example the =C–H band centered at 2962 and 2857 cm^{-1}. Furthermore, a medium strength band at 1460 cm^{-1} was found, which could be assigned to the CH_2 bending vibration or P–C–H group. The weak strength band centered at 1440 cm^{-1} was assigned to phosphorous-phenyl group. In accordance with the materials structure, the OH group stretching band centred at 3740 cm^{-1} is characteristic for terminal silanol groups. By comparison with the pure carrier, after the immobilization of rhodium diphosphine complexes, the intensity of this band decreased.

The acidity of the samples was characterized by FTIR spectroscopy investigating spectra of adsorbed pyridine as probe molecule. The spectra of adsorbed pyridine (Py) after degassing at 200 °C are presented in Fig. 6. Pure all silica materials have an electrically neutral framework and consequently showed no Lewis or Brønsted acidity. After incorporation of aluminum, the

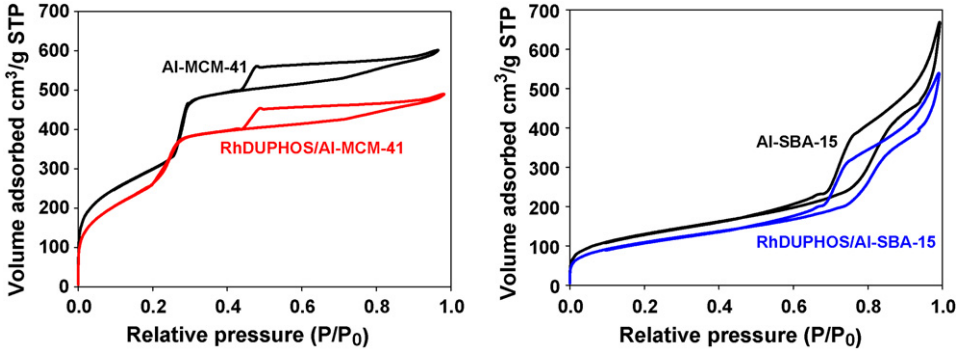

Fig. 4. N_2 sorption isotherms.

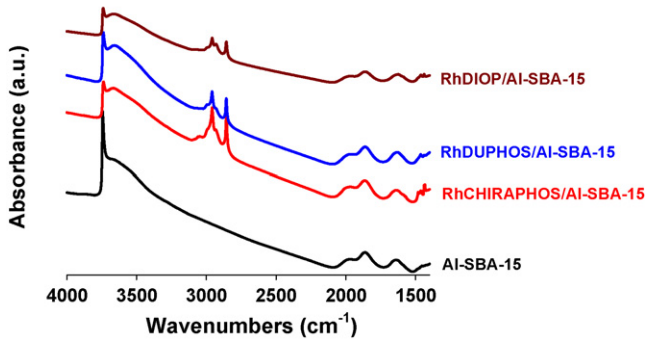

Fig. 5. IR spectra of Al–SBA-15 and rhodium complexes immobilized on Al–SBA-15.

FT-IR spectra of adsorbed Py showed that both Lewis and Brønsted acid sites were created. Al–MCM-41, Al–MCM-48 and Al–SBA-15 exhibited several peaks due to strong Lewis-bound pyridine (1623 and 1456 cm^{-1}), weak Lewis bound pyridine (1577 cm^{-1}) and pyridinium ions on Brønsted acid sites (1546 and 1641 cm^{-1}), while all silica SBA-15 showed only small peaks due to hydrogen bonded pyridine (1446 and 1596 cm^{-1}). Moreover, after the immobilization of the organometalic complex, a slight decrease of the Brønsted and Lewis acidity was observed. This decrease is due to guest/host interaction between the organometallic complex and the solid framework.

Temperature desorption of ammonia was used to characterize the acidity of all silica and aluminated SBA-15, as well as Al–MCM-41 and Al–MCM-48. Fig. 7 presents the results obtained for SBA-15 and Al–SBA-15. Comparison of these TPD curves showed a dramatical increase of the acid strength

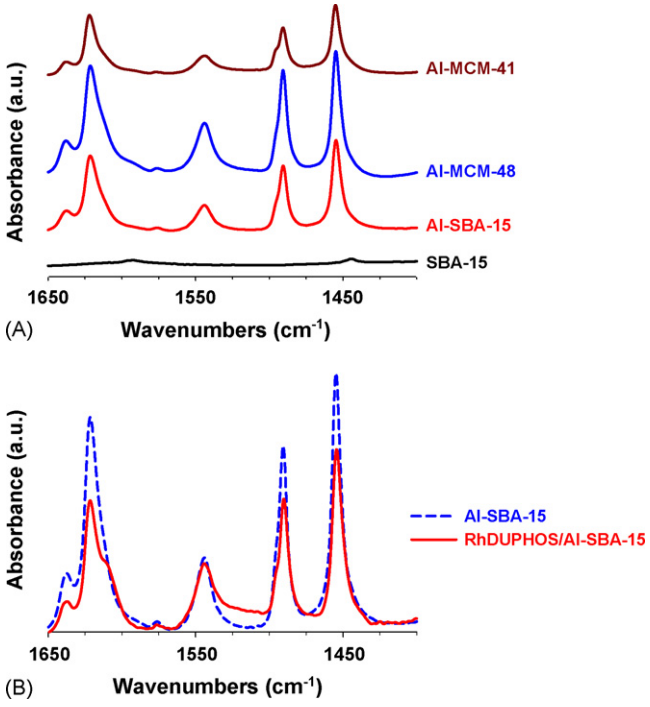

Fig. 6. IR spectra of adsorbed pyridine: (A) pure carriers and (B) Al–SBA-15 and RhDuphos/Al–SBA-15.

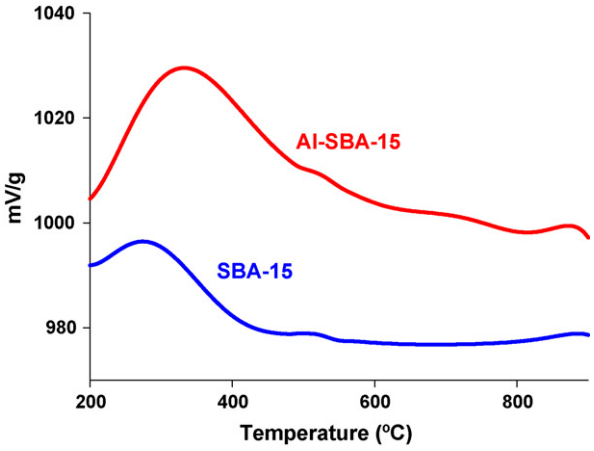

Fig. 7. Temperature programmed desorption of ammonia of SBA-15 and Al–SBA-15.

and amount after alumination. The peaks with maxima at about 300 °C, found for both samples, were due to weakly bond ammonia (physisorbed ammonia, ammonia adsorbed on weak acid sites). The high temperature peak centered at 480 °C, which was much better defined in the case of Al–SBA-15, could be ascribed to ammonia desorbed from strong acid sites. These experiments clearly showed that acid sites were formed after alumination of the surface of the solid.

For Al–MCM-41, temperature-programmed desorption of ammonia showed the presence of weak acidic centers on this type of carrier material. In the case of the immobilized complex, the amount of desorbed ammonia decreased compared to the pure carrier material (Fig. 8). This indicates an interaction of the immobilized complex with acidic sites on the Al–MCM-41. This result was also supported by FT-IR spectroscopy.

Quantitative loading of the organometallic complex was demonstrated with thermal gravimetric analysis. For all immobilized complexes, thermogravimetric and differential scanning calorimetric measurements showed a thermal stability up to 200 °C. In all cases, oxidation of the organic structure

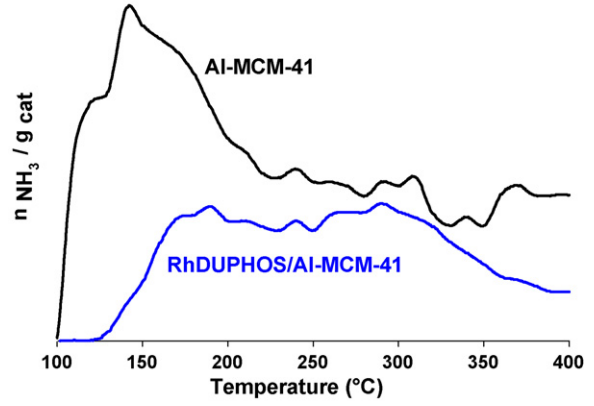

Fig. 8. Temperature programmed desorption of ammonia of Al–MCM-41 and RhDuphos/Al–MCM-41.

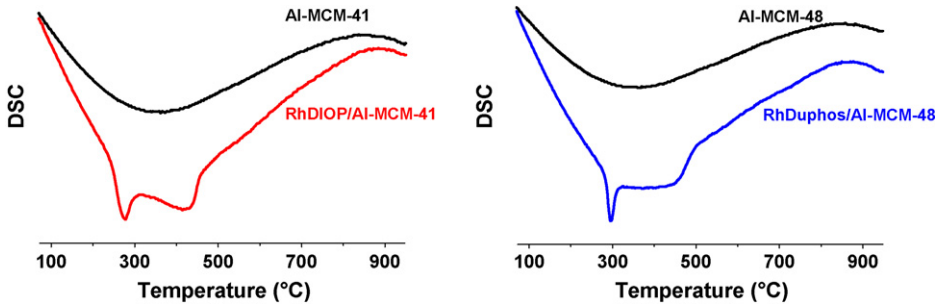

Fig. 9. DSC spectra of Al–MCM-41, RhDiop/Al–MCM-41, Al–MCM-48 and RhDuphos/Al–MCM-41.

took place in two steps, corresponding to about 250 and 400 °C, respectively (Fig. 9). The loss of weight of ca. 3–5 wt.% caused by burning of the complex was consistent with the content determined by chemical analysis. The oxidation of the pure carriers showed no characteristic peak.

In order to elucidate the chemical structure of the immobilized rhodium diphosphine complexes, MAS-NMR of the pure Al–SBA-15 carrier, the homogeneous complexes, and the immobilized complexes have been recorded. Due to the low content of immobilized complex, the ^{13}C and ^{1}H resonance signals were too weak for quantitative interpretation. The pure carrier and immobilized complexes showed not significantly different spectra for the ^{27}Al and ^{29}Si nuclei. Therefore, the interpretation of a chemical shift is risky.

^{31}P MAS NMR spectra of the solid homogeneous CODRhChiraphos complex and the same complex immobilized on Al–SBA-15 are depicted in Fig. 10. The homogeneous complex gave a strong signal at 59 ppm and two weaker ones at 30 and 75 ppm due to trace amounts of oxidic impurities. The MAS NMR spectrum of the immobilized CODRhChiraphos complex showed only a single signal at 71 ppm. The absence of signals of the homogeneous complex and of the free phosphine ligand was an indication that the phosphine ligand was completely coordinated to the rhodium. Similar results were obtained for CODRhChiraphos immobilized ona Al–MCM-41 or Al–MCM-48. The immobilization of this rhodium Chiraphos

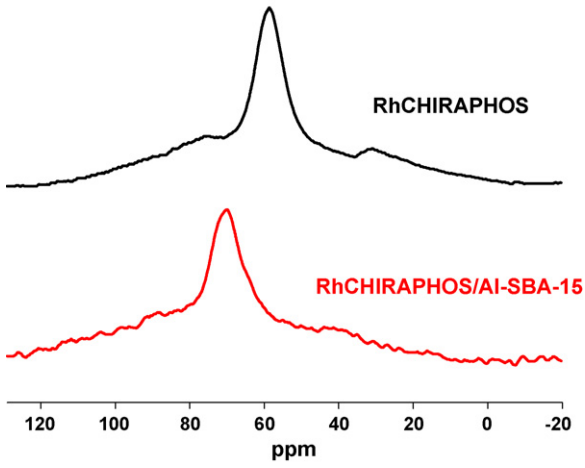

Fig. 10. ^{31}P MAS NMR of (a) homoegeneous RhChiraphos and (b) RhChiraphos immobilized on Al–SBA-15.

complex led to a shift of the ^{31}P signal of 12 ppm to lower magnetic field compared to the homogeneous complex as the result of the interaction of the guest complex with the surface of the Al–SBA-15 host, more specifically to the interaction with a Lewis acidic center on the surface, which withdraws electrons from the rhodium metal or the phosphine ligand, and thus lowers the electron density.

The rhodium complexes used consisted of a chiral diphosphine and a cyclooctadiene ligand. There could be several forces involved in the bonding of the complex to aluminum containing mesostructured materials. For example, an electrostatic interaction of the cationic complexes with the anionic framework of the mesoporous material could occur. A similar mechanism was reported for the immobilization of manganese complexes on Al–MCM-41 [33]. Furthermore, direct bridging of the rhodium to surface oxygen of the mesoporous walls has also been observed and could occur after cleavage of the diene complex during the hydrogenation reaction [34]. However, no evolution of cyclooctadiene during the immobilization reaction could be observed, and FT-IR spectra of the filtrate obtained after the impregnation did not contain bands attributable to free cyclooctadiene.

3.1. Catalytic results

Several diphosphine ligands have been applied and the corresponding complexes have been tested for the immobilization. The activity of the different free and immobilized catalysts in several enantioselective hydrogenation reactions was investigated (Fig. 11). In blank reactions using the parent materials no reactions took place, and over Rh supported on mesostructured materials no enantiomeric excess was observed, although conversions of up to 99% were found. Moreover, for all hydrogenation experiments the chemical selectivity was 100%. No side products were observed.

Table 4 presents the results obtained with free and immobilized RhDuphos and RhBPE. As observed, all reactionS performed with complete conversion and 100% selectivity. The enatioselectivity obtained for these complexes immobilized on Al–MCM-41 or Al–MCM-48 is close to or higher than the enantioselectivity of the free complexes, while the e.e. values obtained for the complexes immobilized on Al–SBA-15 were lower then the ones obtained in homogeneous catalysis. Al–MCM-41 and Al–MCM-48 have mesopores with a diameter of 3–3.5 nm, while the postaluminated SBA-15 presented pores

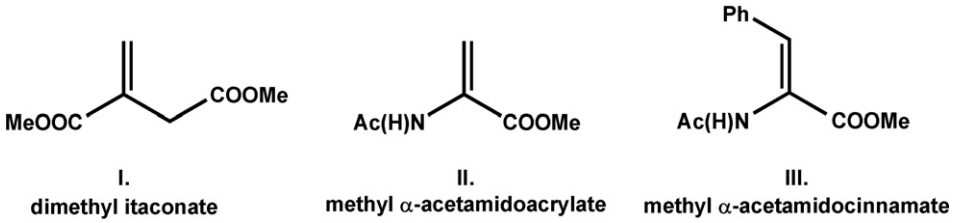

Fig. 11. Substrates used in enantioselective hydrogenation.

Table 4
Catalytic performance of free and immobilized RhDuphos and RhBPE

Complex	Substrate	Carrier	Conversion (%)	Selectivity (%)	e.e. (%)
	I	–	99	100	94
		Al–MCM-41	99	100	92
		Al–MCM-48	99	100	98
		Al–SBA-15	99	100	89
RhDUPHOS	II	–	99	100	94
		Al–MCM-41	99	100	97
		Al–MCM-48	99	100	97
		Al–SBA-15	99	100	93
	III	–	99	100	96
		Al–MCM-41	99	100	99
		Al–MCM-48	99	100	98
		Al–SBA-15	99	100	90
	I	–	99	100	92
		Al–MCM-41	99	100	84
		Al–MCM-48	99	100	92
		Al–SBA-15	99	100	84
RhBPE	II	–	99	100	90
		Al–MCM-41	99	100	94
		Al–MCM-48	99	100	95
		Al–SBA-15	99	100	82
	III	–	99	100	89
		Al–MCM-41	99	100	84
		Al–MCM-48	99	100	82
		Al–SBA-15	99	100	76

Reaction conditions: 3 bar H_2 pressure, r.t., 24 h, 0.05–0.2 M substrate, MeOH, S/C = 1000.

with a diameter of 9.2 nm. This behavior might be due to the higher steric constraints presented inside of the mesoporous systems of Al–MCM-41 and Al–MCM-48.

Fig. 12 shows the catalytic performance of Al–SBA-15 based RhChiraphos, RhProphos and RhDiop for asymmetric hydrogenation of dimethyl itaconate (**I**) and methyl α-acetamidoacrylate (**II**). Over these immobilized complexes enantioselectivities of 62–79% at 85–96% conversion were obtained, while the homogeneous counterparts showed 86–91% e.e. at quantitative conversion.

The immobilized catalysts were also employed at high substrate/catalyst ratios. The complexes immobilized on Al–MCM-41 and Al–MCM-48 were successfully used at substrate/catalyst ratios of 2000–6000 with high to complete conversion and no loss of enantioselectivity relative to lower substrate/catalyst ratios (Fig. 13). For example, when RhDuphos/Al–MCM-48 was employed for hydrogenation of dimethyl itaconate at S/C = 6000, 94% conversion and 98% e.e. were obtained. The result corresponds to a TON of 5630. However, Al–SBA-15 based rhodium diphosphine complexes showed bad results for high substrate/catalyst relative to the lower ones. The M41S solids were synthesized as aluminum containing materials, while the SBA-15 material used here was aluminated by post-synthesis. The difference as-synthesis/post-synthesis alumination might affect the guest/host interaction and influence the activity of the immobilized complexes at high substrate/catalyst ratio. It is also possible that stronger constraints in the smaller pore sized M41S materials compared

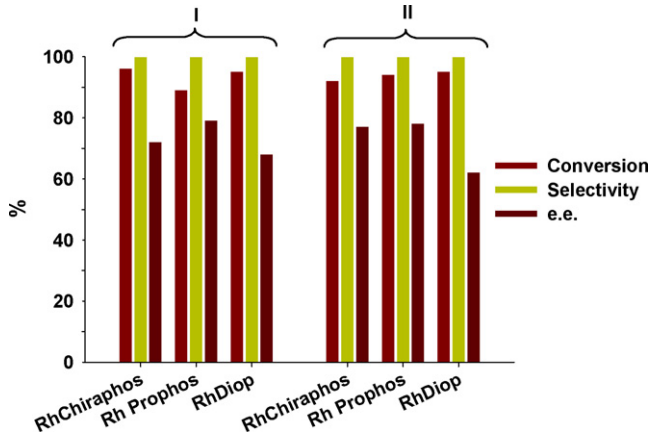

Fig. 12. Hydrogenation of dimethyl itaconate and methyl α-acetamido acrylate over RhPP/Al–SBA-15 (same reaction conditions as for Table 4).

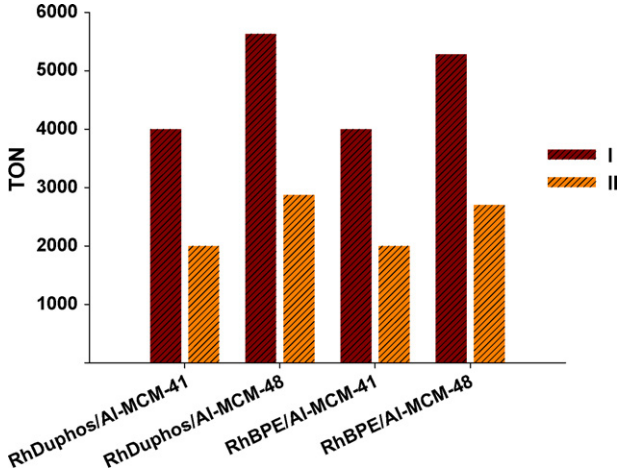

Fig. 13. TON obtained at high substrate/catalyst ratios (3 bar H_2 pressure, r.t., 24 h, 0.05–0.2 M substrate, S/C = 2000–6000).

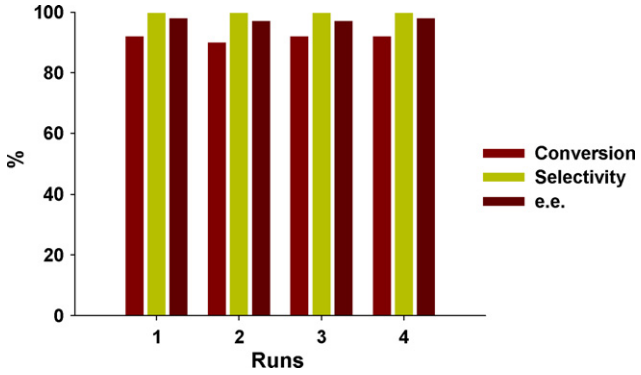

Fig. 14. Recyclability test.

with the SBA-15 cause such an effect. Right now, we have no clear understanding of these results.

The recyclability of the immobilized rhodium diphosphine complexes was tested using standard procedures. It was found that these catalysts could be recycled four times without any loss of activity and chemo- or enatioselectivity. Fig. 14 presents the reuse of RhDuphos/Al–MCM-48 in hydrogenation of dimethyl itaconate (**I**) at S/C ratio of 6000. For this reaction, the turnover number over the four cycles was >20,000.

In order to prove that the reaction was catalyzed heterogeneously and to exclude the possibility of leaching and homogeneous catalysis, the reaction mixture was separated from the catalyst before complete conversion occurred (hot filtration test) [35]. For the dimethyl itaconate hydrogenation, removal of the CODRhDuphos immobilized on Al–SBA-15 effectively stopped the reaction after 6 h. After 24 h the conversion of the filtered sample remained at 42%, whereas the original batch with catalyst was converted completely. This proved that no homogeneous catalysis took place. ICP AES analysis of the filtered reaction solution showed traces of rhodium, phosphorus, silicon, and aluminium, in relative amounts corresponding with the composition of the heterogeneous catalyst, indicating that this loss occurred by attrition of the Al–SBA-15 rather then by leaching of the complex, because the mixture was vigorously stirred.

4. Conclusion

Heterogeneous chiral catalysts were prepared from chiral rhodium diphosphine complexes and aluminum containing MCM-41, MCM-48 and SBA-15. The complexes were bonded to the carrier by the interaction of the cationic rhodium of the organometallic complex with the anionic host framework, as well as between Al Lewis acid sites and P Lewis basic sites. This immobilization method is effective and simpler than covalent bonding of guest molecules.

These new heterogeneous catalysts were applied for asymmetric hydrogenation of dimethyl itaconate, methyl α-acetamidoacrylate and methyl α-acetamidocinnamate. The immobilized catalysts showed high activities and excellent chemo- and enantioselectivities, achieving up to 98% e.e., at >99% conversion and 99% selectivity. The obtained results indicated that the stereochemistry of the product was mainly dictated by the chirality of the diphosphine ligands.

The recyclability of rhodium diphosphine complexes immobilized on aluminum containing mesostructured materials was demonstrated using standard procedures. The catalysts could be reused at least four times without any loss of activity, obtaining TONs larger than 20,000. The high activities observed with these supported organometallic complexes, plus the fact that the high activity is maintained upon reuse of the catalysts, indicated that these are truly heterogeneous counterparts of homogeneous transition metal complexes.

Acknowledgments

The authors are very grateful for the financial support from the Sonderforschungsbereich SFB 380 of the Deutsche Forschungsgemeinschaft (DFG). Johnson Matthey PLC Catalysts & Chemicals Division is acknowledge for a sample of $[CODRhCl]_2$.

References

[1] S.C. Stinson, Chem. Eng. News 79 (2001) 79.
[2] A.M. Rouhi, Chem. Eng. News 81 (2003) 45.
[3] A.M. Rouhi, Chem. Eng. News 82 (2004) 47.
[4] I. Ojima (Ed.), Catalytic Asymmetric Synthesis, 2nd ed., Wiley–WCH, New York, 2000.
[5] H.U. Blaser, F. Spindler, M. Studer, Appl. Catal. A 221 (2001) 119.
[6] Nobel Lectures, Angew. Chem. Int. Ed. 41 (2002) 998.
[7] H. Brunner, W. Zettlmeier (Eds.), Handbook of Enantioselective Catalysis, VCH, Weinheim, 1993.
[8] J.M. Brown, in: E.N. Jacobsen, A. Pfaltz, H. Yamamoto (Eds.), Comprehensive Asymmetric Catalysis, Springer, Berlin, 1999, p. 121.
[9] H.U. Blaser, Adv. Synth. Catal. 344 (2002) 17.
[10] A. Nagel, J. Albrecht, Topics Catal. 5 (1998) 3.
[11] H.U. Blaser, C. Malan, B. Pugin, F. Spindler, H. Steiner, M. Studer, Adv. Synth. Catal. 345 (2003) 103.
[12] H. Kagan, N. Langlois, T.-P. Dang, J. Organomet. Chem. 90 (1975) 353.
[13] W.S. Knowles, M. Sabacky, B.D. Vineyard, J. Chem. Soc. (1972) 10.
[14] F.J. Waller, Chem. Ind. 89 (2003) 1.
[15] H.U. Blaser, B. Pugin, M. Studer, in: D.E. de Vos, I.F.J. Vankelecom, P.A. Jacobs (Eds.), Chiral Catalyst Immobilization and Recycling, Wiley–VCH, Weinheim, 2000, p. 1.
[16] B. Pugin, H.U. Blaser, in: E.N. Jacobsen, A. Pfaltz, H. Yamamoto (Eds.), Comprehensive Asymmetric Catalysis I–III, vol. 3, Springer, Berlin, Heidelberg, New York, 1999, p. 1367.
[17] S. Braese, F. Lauterwasser, R.E. Ziegert, Adv. Synth. Catal. 345 (2003) 869.
[18] D.E. Bergbreiter, Chem. Rev. 102 (2002) 3345.
[19] C.E. Song, S.-G. Lee, Chem. Rev. 102 (2002) 3495.
[20] D.E. de Vos, M. Dams, B.F. Sels, P.A. Jacobs, Chem. Rev. 102 (2002) 3615.
[21] S. Anderson, H. Yang, S.K. Tanielyan, R.L. Augustine, Chem. Ind. 82 (2001) 557.
[22] D.E. de Vos, B.F. Sels, P.A. Jacobs, Adv. Catal. 46 (2001) 1.
[23] W.F. Hoelderich, H.H. Wagner, M.H. Valkenberg, R. Soc. Chem. 266 (2001) 76 (Special Publication).
[24] M.H. Valkenberg, W.F. Hölderich, Catal. Rev. 44 (2002) 321.
[25] J.S. Beck, J.C. Vartulli, W.J. Roth, M.E. Leonowicz, C.T. Kresge, K.D. Schmitt, C.T.-W. Chu, D.H. Olson, E.W. Sheppard, S.B. McCullen, J.B. Higgins, J.L. Schlenker, J. Am. Chem. Soc. 114 (1992) 10834.
[26] D. Zhao, J. Feng, Q. Huo, N. Melosh, G.H. Frederickson, B.F. Chmelka, G.D. Stucky, Science 279 (1998) 548.

[27] D. Zhao, Q. Huo, J. Feng, B.F. Chmelka, G.D. Stucky, J. Am. Chem. Soc. 120 (1998) 6024.
[28] H.H. Wagner, H. Hausmann, W.F. Hölderich, J. Catal. 203 (2001) 150.
[29] A. Crosman, W.F. Hoelderich, J. Catal. 232 (2005) 43.
[30] Z. Luan, M. Hartmann, D. Zhao, W. Zhou, L. Kevan, Chem. Mater. 11 (1999) 1621.
[31] M. Cheng, Z. Wang, K. Sakurai, F. Kumata, T. Saito, T. Komatsu, T. Yashima, Chem. Lett. (1999) 131.
[32] M. Busio, J. Jaenchen, J.H.C. van Hooff, Micropor. Mater. 5 (1995) 211.
[33] S.S. Kim, W. Zhang, T.J. Pinnavaia, Catal. Lett. 43 (1997) 149.
[34] A. Janssen, J.P.M. Niederer, W.F. Hölderich, Catal. Lett. 48 (1997) 165.
[35] H.E.B. Lempers, R.A. Sheldon, J. Catal. 175 (1998) 62.